Stopping power of WDM for protons at low energies

M.D. Barriga-Carrasco, J. Vázquez-Moyano, F. Chacón-Rubio, J. Chacón-Gijón

E.T.S.I. Industrial, Universidad de Castilla-La Mancha, Ciudad Real 13071, Spain

Introduction

WDM regime covers the condensed matter regime categorized by a wide range of electron temperatures, 1-100 eV, and pressures from ambient to many Mbar, covering ionized fluids at the confluence of condensed matter physics, plasma physics and dense liquids [1]. Currently, most of laser-generated plasmas go through WDM state at some point. Hence, experimental measurements and numerical simulation data provide a useful tool to distinguish between stopping power models of the WDM, which are highly uncertain [2]. However, precise measurements of plasma conditions and energy loss in WDM are still hard to achieve. In this work, calculations performed with the hydrodynamic code MULTI-fs [3] and with our stopping power model, as well as other models, will be carried out in a simulated experiment. The hydrodynamic simulation results are used to calculate the stopping power of the WDM electrons by means of theoretical models.

Hydrodynamic simulations

Some input parameters considered to perform the numerical simulation with MULTIfs code are extracted from those that can be achieved with the petawatt laser systems available in Europe, like PHELIX, DRACO, or VEGA-II, in order to obtain the most realistic plasma state as possible in the simulated experiment. Simulation setup parameters apply for the two main actors involved in the experiment: laser and target specifications. Simulation results are presented in this section, more precisely. Electron temperature, mass density, ionization degree, coupling and reduced temperature curves are shown. In Fig. 1 electron temperature vs plasma areal density curves are represented. It is evidenced that the later the time is selected, the lower the electron temperature is, as the target begins to cool down with time. Greater

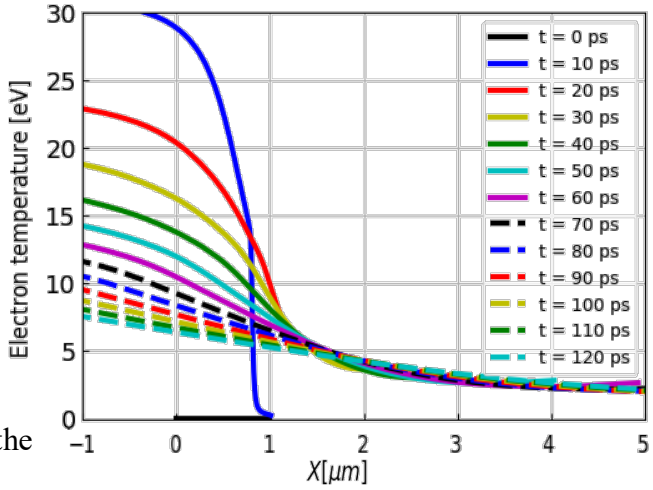

Figure 1: Electron temperature as a function of depth at different expansion times.

temperatures occur at the left part of the target as it is the zone where the laser hits, producing steep gradients at early times.

Stopping power model

This section describes the stopping power model used in this work. The stopping power calculations are based on the plasma parameters previously simulated and, they are necessary for the estimation of the projectile energy loss in the plasma. The total stopping power of partially ionized matter can be estimated from the contributions of free and bound electrons [4, 5].

$$\frac{dE}{dx} = \left(\frac{dE}{dx}\right)_{fe} + \left(\frac{dE}{dx}\right)_{be} = \frac{4\pi Z_p^2}{v_p^2} n_i (qL_{fe} + L_{be}). \quad (1)$$

where Z_p is the effective charge state of the projectile [6, 7, 8], q is the plasma ionization, v_p is the projectile velocity, n_i is the ion density of the plasma and L_{fe}, L_{be} are the free and bound stopping numbers respectively. The free electron density can be calculated as $n_{fe} = n_i q$. The free electronic contribution is calculated by the dielectric formalism [9, 10].

Bound electrons

For a wide range of conditions, including WDM, the plasma is not fully ionized and bound electrons need to be considered for stopping power calculations. Only few models include bound electron contribution explicitly, our present model and other previous simple models. Our present model SLPA [11] relies on two assumptions. The first one is the shellwise consideration, which describes the stopping power of projectiles within each *nl* sub-shell of target bound electrons independently, where *n* and *l* are the principal and azimuthal quantum numbers, respectively. The second assumption, LPA, extends the dielectric formalism to deal with atomic bound electrons as a free-electron gas of local density. The electron density of the shell, $\rho_{nl}(r)$, and the binding energy are the only inputs for SLPA. For atoms, they can be obtained from the Hartree-Fock wave functions. The combination of both assumptions is what is called SLPA.

Fig. 2 shows the bound electron stopping power contribution of these models for a carbon plasma at T = 20 eV and ionization q = 2.31. SRIM [12] results for the solid case (T = 0, q = 0) is also plotted for comparison. The LSS in Mehlhorn model diverges very quickly for light projectiles and target atoms and is valid only in an approximate range of proton energy Ep < 0.03 MeV. To avoid this divergence, a cutoff has been imposed producing the sharp peak in

the union with the Bethe stopping. While the agreement at high energies is fairly good, at low energies, there are severe discrepancies between these models. This regime is still not completely understood, and the variety of considerations made in this region result in large discrepancies observed between models. Different approximations of the ionization potential would have only a small effect on the stopping power. As the SLPA model is the most complete model for the treatment of bound electrons stooping among those here considered, it will be used for the total stopping power and energy loss calculations in next section.

Energy loss results

Usually, the experiments give energy loss data more than stopping power values, then it is interesting to calculate the energy loss from the last stopping power models. It is not trivial as the WDM changes its density, temperature, and ionization with time. Then, the energy loss will be calculated for each instant of time in Fig. 3. In this figure, the solid case is a case with constant conditions that serves as a reference. In the case of WDM, the free and bound results are time varying due to the time evolution of the target conditions. We will use only our present stopping model and the T-Matrix model for the energy loss calculations, though the same procedure can be done for the other stopping models.

For the WDM case, the energy loss is clearly higher than that for the solid case, this effect is known as enhanced stopping power. Notice that the energy loss grows with time in WDM. At early times, both temperature and ionization present high values. Despite the high ionization, the high temperatures cause a significant reduction of the free contribution to the stopping power [13]. As the plasma begins to expand, temperature and ionization decrease. This lower temperature makes the free electron contribution be higher, despite the diminishing of the ionization. As ionization diminishes slowly with time, the bound contribution increases slowly too. Then, the main reason for the overall increase of the total energy loss is the effect of lower temperatures in the free electron stopping power, see Fig.3.

Conclusions

As can be seen from the stopping graph Fig. 2 it is needed an experiment with energies closer to the Bragg peak to establish a clear distinction between WDM models. With the present models a total energy loss of up to a 100% above the solid case has been estimated for carbon WDM at initial proton energy of 0.1 MeV, as it is shown in Fig. 3.

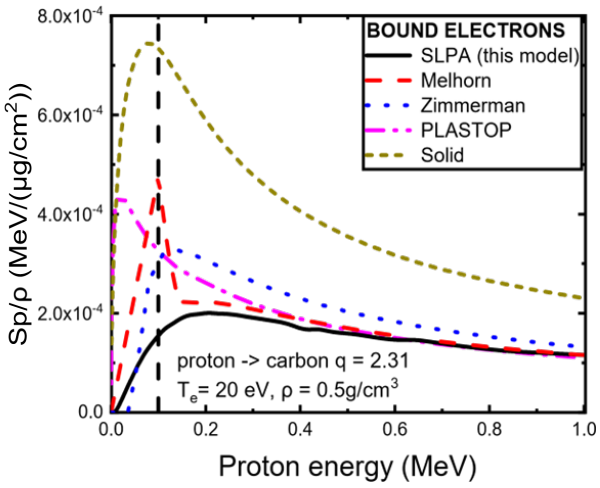

Figure 2: Comparison of bound electron stopping power models for a carbon WDM

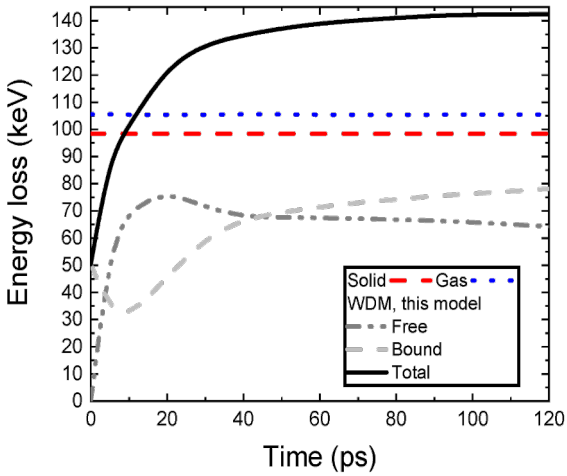

Figure 3 Energy loss of protons when passing through carbon WDM described in Fig. 1.

It must be emphasized that in this work, the stopping power has been calculated with much more precision than in any previous works thanks to the detailed results from the hydrodynamic code for each instant of time and position. This work could be used in a future to design an experiment to distinguish definitively between different possible theoretical models of the stopping power of WDM at Bragg peak projectile energies.

Acknowledgements

This work was financed by the Junta de Comunidades de Castilla-La Mancha under Contract No. SB-PLY/19/180501/000105 (FEDER) and the Spanish Government under Contract No. PID2021-127381NB-I00.

References

[1] T. Dornheim, S. Groth, and M. Bonitz, Physics Reports 744 (2018), pp. 1–86.

[2] Yun Liu et al., Phys. Rev. E 103.063215 (2021).

[3] J. Meyer-ter-Vehn R. Ramis K. Eidmann and S. Hüller. Comp. Phy. Commun.183 (2011), pp. 637–655.

[4] D. Casas, M. D. Barriga-Carrasco, and J. Rubio. Physical Review E 88.3 (2013), p. 033102.

[5] M. D. Barriga-Carrasco and D. Casas, Laser and Particle Beams 31 (2013), pp. 105–111.

[6] M. D. Barriga-Carrasco. Phys. Rev. E 88 (2013), p. 043107.

[7] M. D. Barriga-Carrasco et al. Phys. Rev. E 93 (2016), p. 033204.

[8] J. Braenzel et al. Physical Review Letters 120.18 (2018) p. 184801,

[9] M. D. Barriga-Carrasco and G. Maynard. Laser and Particle Beams 24.1 (2006), pp. 55–60.

[10] Manuel D. Barriga-Carrasco. Laser and Particle Beams 28.2 (June 2010), pp. 307–311.

[11] M. D. Barriga-Carrasco, F. Chacón-Rubio, and C. C. Montanari, European Phys. Journal Plus 137.3 (2022).

[12] J. F. Ziegler, J.P. Biersack, and U. Littmark. Pergamon Press, London (1985).

[13] L. González-Gallego, M.D. Barriga-Carrasco, and J. Vázquez-Moyano, Phys. Plasmas 28.043103 (2021).